İSTANBUL UNIVERSITY
CERRAHPAŞA

ORIGINAL ARTICLE
Electrica 2023; 23(2): 385-396

Load Adaptive PID-Aided Asymmetrical Voltage Cancellation Controller-Based Induction Heating System With Improved Power Factor

Anand Kumar, Chandan Kumar

Department of Electrical and Electronics Engineering, Sarala Birla University, Ranchi, Jharkhand, India

Cite this article as: A. Kumar and C. Kumar, "Load adaptive PID-aided asymmetrical voltage cancellation controller-based induction heating system with improved power factor," *Electrica*, 23(2), 385-396, 2023.

ABSTRACT

In a multiple load induction heating (IH) system, the effective voltage across particular load changes during different loading conditions. Thus, the quality of heating across the IH load degrades. Furthermore, in any IH system, a high-frequency (HF) inverter with a high switching frequency makes HF components that flow back toward the utility side and distort the waveform of the current. The constant input voltage to the IH loads with quality input current is an essential condition to generate uniform heating. To accomplish this, a load adaptive proportional integral derivation (PID)-aided asymmetrical voltage cancellation control scheme is proposed to maintain a constant voltage profile across the IH load under variable load conditions. A boost power factor correction converter has been used as a front-end converter followed by a HF full-bridge series resonant inverter to improve the utility power factor. The proposed IH system ensures unity power factor operation along with a constant voltage profile across the load, and it has been validated through the MATLAB/Simulink environment. Also, a prototype has been developed using embedded control, and its dynamic behavior has been studied under multiple IH loads. The obtained simulation and experimental results confirm the effectiveness of the proposed IH system under the aforesaid control scheme.

Index Terms—Asymmetrical voltage cancelation, boost PFC converter, embedded control, full-bridge series resonant inverter, multi-load IH system, zero voltage switching.

Corresponding author:
Anand Kumar

E-mail:
anandsingh1025@gmail.com;
anand.kumar@sbu.ac.in

Received: August 16, 2022

Accepted: January 11, 2023

DOI: 10.5152/electr.2023.22142

I. INTRODUCTION

In the past few years, induction heating (IH) technology is widely being applied in industrial, medical, and domestic application due to its astonishing advantages in terms of its efficiency, less heating time, and cleanness as compared to other approaches of heating method [1, 2]. High-frequency (HF) oscillating current is the imperative requirement in modern IH technology to generate HF eddy current in IH loads [3]. Along with it, the heating effect in IH loads must be appropriate as well as efficiently controlled to get the desired temperature level to the workpiece. To do this, resonant inverters play a vital role in the IH system [4, 5]. Numerous resonant inverters have traditionally used a variety of control techniques to regulate the output voltage [6]. The most economical option is a series resonant inverter fed by a voltage source, but power control requires a variable direct current (DC) input voltage. For the variation in DC voltage, a bridge rectifier with a DC link capacitor has traditionally been used. This had issues with cost, supply current, and size, with higher harmonic distortion [7-10]. Modern domestic IH is mostly equipped with voltage-fed class D amplifier and half-bridge topology based on the series resonant tank due to its good balance between performance and cost-effective solution [11, 12]. But only low-power applications can use these converters, and they are unable to maintain zero voltage switching (ZVS) conditions properly. Different power control techniques have been developed to control the output power, which results in generating a regulated heating effect in an IH load or workpiece, such as pulse width modulation (PWM), pulse frequency modulation, and pulse density modulation (PDM) [13-15]. In the PWM technique, switching frequency and duty cycle variation are used to control the output power of the resonant inverter. In the PDM technique, variations in conduction and non-conduction period of the switches are used to regulate the output power. But it gives discontinuous power to the IH load and can be applied only for low-power ranges [16]. Commonly, varying switching frequency method is used to control the output power in many resonant inverters. But this method has several demerits like more

electromagnetic interference (EMI), complex design of filtering components, and poor utilization of magnetic components [17]. These drawbacks can be resolved by using a fixed-frequency control technique which has been classified as phase shift, asymmetrical duty cycle, and asymmetrical voltage cancellation (AVC) techniques [18-20]. However, these methods do not seem to maintain the ZVS/ZCS condition under variable load or power requirement. These methods enable to modify the output power, but for the dynamic nature of the IH system or in multi-coil/load IH system, usually a closed-loop output power control technique is needed. This technique obtains a recurrent and precise output power for a specified reference irrespective of the difference in load or input voltage.

Currently, the multi-coil/load IH system has received a lot of attention, but it is still widely used even though it lacks a clear combination of inverters and power control methods [21, 22]. It has been observed that the main barrier in the multi-coil/load IH system is that effective impedance varies as variation in alignment between the workpiece and IH coil, frequency, and temperature [23, 24]. Owing to this, the applied effective voltage to the IH load decreases. The applied effective voltage also decreases due to a change in exogenous parameters (that is load parameters). Enabling constant effective or output voltage across particular IH load plays a vital role in the modern multi-coil/load IH system in order to increase its efficiency. Currently, in the multi-coil/load IH system, the problem is not only limited to design new resonant inverters topology but to improve the power control strategies in which power must be separately maintained constant or regulated [25-27].

A closed-loop load adaptive (LA) PID-aided AVC control scheme described in this article can be used to solve the aforementioned issues. This proposed scheme not only maintains the ZVS condition but also improves input power factor as well as maintains constant output voltage irrespective of variation in load parameters or input variation.

The full-bridge series resonant inverter (FB-SRI) is chosen in this work because it enables numerous control possibilities [26, 28-30], shown in Fig. 1. This FB-SRI simultaneously powers multi-coil/loads, but in this work, only two IH loads are being considered. Change in load parameters is achieved by a step change in one load which causes the dip in voltage to another load. Additionally, a boost power factor correction (PFC) converter is used as a front-end converter which corrects the input PF and improves the total harmonic distortion (THD) along with the reduction in the HF component. The proposed multi-coil/load IH system has been validated through a MATLAB/Simulink environment. Additionally, the experimental setup has been implemented where the control scheme is developed using a low-cost Arduino 2560 embedded system. Good agreement has been found between simulation and the experimental results. Consequently, the performance and efficiency of the proposed closed-loop IH system are significantly improved.

The remaining part of this work is divided into four sections. In Section II, a proposed closed-loop AVC-based IH system has been discussed. Analysis of FB-SRI under the AVC technique has been described in Section III. The performance of the proposed IH system under variable load has been studied in different aspects which is given in Section IV. Moreover, implementation of experimental setup is given in Section V. Finally, conclusion is made in Section VI.

II. PROPOSED CLOSED-LOOP PID-AIDED ASYMMETRICAL VOLTAGE CANCELLATION-BASED INDUCTION HEATING SYSTEM

The proposed IH system comprised of a diode bridge rectifier, a boost PFC converter, an HF FB-SRI, and dual IH loads is shown in Fig. 2. Here, the 1-ø AC supply (V_s) is converted to DC supply (V_{DC}) by means of a full-bridge operation. Thereafter, the output DC voltage (V_{DC}) is given to the boost PFC converter to defend the HF harmonic component, which comes from the HF operation of FB-SRI as well as to improve the input power quality. Now, the output of the boost PFC converter that is DC link voltage (V_{DCl}) is given to the FB-SRI which supplies HF current to the IH coil, so that IH load/workpiece gets heated. Two IH loads have been used, which is modeled as a series connection of equivalent resistance (R_{eq}) and inductance (L_{eq}). A common resonating capacitor (C_{cr}) is used to achieve series resonant condition for dual IH loads. In this work, two independent controllers have been used, one for boost PFC converter and other for FB-SRI, respectively, which is as follows.

A. Description of Control Strategy for a Boost Power Factor Correction Converter

The controller for the boost PFC converter has been designed and aimed to achieve unity power factor operation of the utility mains, thus eliminating the HF component at the input side. The control scheme for boost PFC is shown in Fig. 3. Firstly, the output voltage of the boost PFC (V_{DCL}) is compared with the reference voltage (V_{ref}), and the generated error (e_v) is applied to the proportional integral (PI)

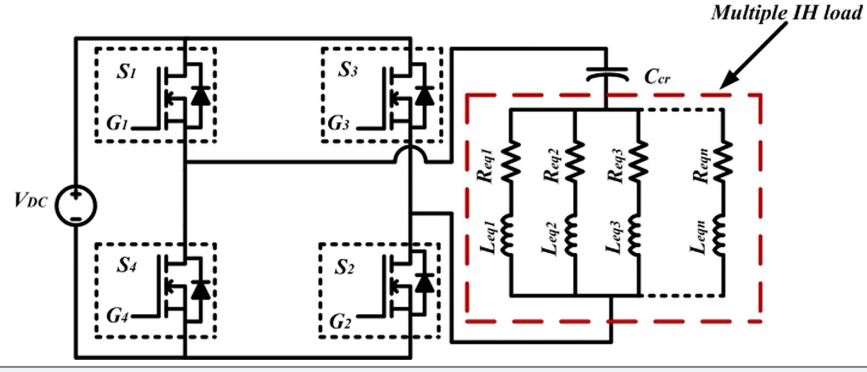

Fig. 1. Full-bridge series resonant inverter for multiple induction heating (IH) loads.

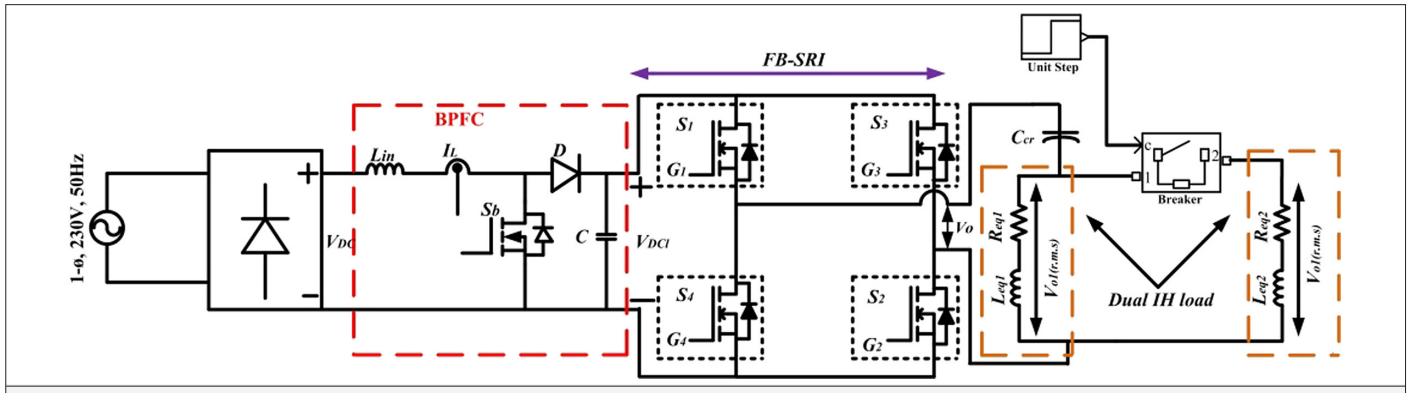

Fig. 2. Proposed induction heating (IH) power supply system. FB-SRI, full-bridge series resonant inverter.

controller, which is a voltage controller (G_{CV}). This V_{ref} is nothing but the output voltage across the IH load. Thereafter, an input reference current (i_{ref}) is generated by multiplying the output of the voltage controller (i.e., I_{ref}) with a rectified unitary template sine wave voltage ($V_{s(t)}$), which is as follows:

$$V_{s(t)} = \frac{|V_s|}{V_m} = |\sin \omega t| \tag{1}$$

where $V_s = V_m \sin \omega t$ and V_m is the maximum voltage of the input supply.

The PI current controller (G_{CI}) now compares input current reference (i_{ref}) to inductor current (I_L) and generated error (e_i), resulting in V_{cont}. Finally, this V_{cont} is compared with the HF triangular signal (V_{tri}) to get the switching signal for the switch, S_b. A state-space averaging technique has been used to analyze and design this control scheme, which is as follows:

$$L_{in} \frac{dI_L}{dt} = V_m |\sin \omega t| - (1 - D(t)) V_{ref} \tag{2}$$

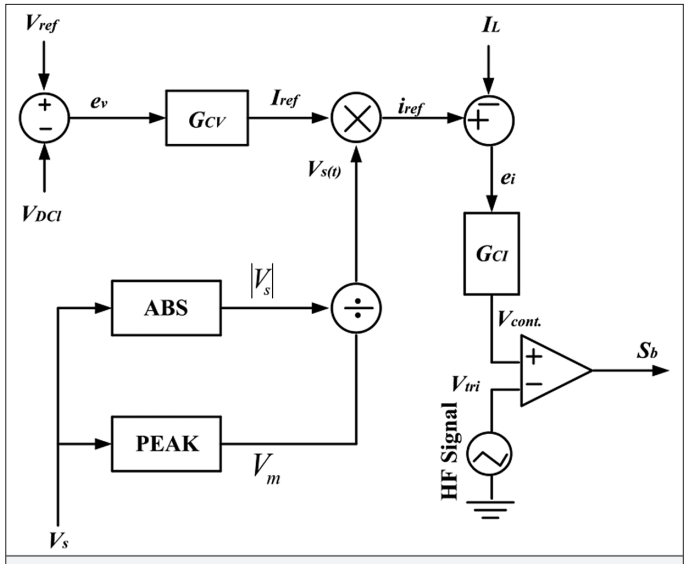

Fig. 3. Controller for a boost power factor correction converter. HF, high frequency.

where L_{in} and $D(t)$ are the boosting inductor and duty cycle function of the pulse width modulator, which can be expressed as:

$$D(t) = \frac{V_{cont}}{V_{tri}} \tag{3}$$

where V_{tri} is the maximum voltage of the HF triangular signal.

On putting the value of $D(t)$ from (3) in (2), we can get

$$\frac{dI_L}{dt} = \frac{V_m \sin \omega t}{L_{in}} - \frac{V_{ref}}{L_{in}} + \frac{V_{ref}}{L_{in} V_{tri}} V_{cont} \tag{4}$$

From Fig. 3, the Laplace form of V_{cont} is as

$$V_{cont}(s) = \{I_{ref}(s) - I_L(s)\} G_{CI}(s) \tag{5}$$

On solving (4) and (5), inductor current (I_L) in Laplace form can be written as:

$$I_L(s) = \frac{|V_m|(s)}{sL_{in}(1+G(s))} - \frac{V_{ref}}{s^2 L_{in}(1+G(s))} + \frac{G(s)}{1+G(s)} I_{ref}(s) \tag{6}$$

where $G(s) = \frac{V_{ref}}{sL_{in}V_{tri}} G_{CI}(s)$ (7)

and $G_{CI}(s) = K_p + K_i/s$ (8)

K_p and K_i are the proportional and integral gains, respectively.

According to (6), the control loop can be considered of as being disturbed by the input voltage's absolute value. V_{ref} can also be assumed of as a continual disturbance. In the face of these disturbances, the control's goal is to ensure that the inductor current follows a sinusoidal reference current. A PI controller $G_{CI}(s)$ is used in the design and implementation of the traditional control method and is also the one that is most frequently used in real-world applications. In this way, the input reference current (I_R) is inherently synchronized and is always proportional to the line voltage, which is the condition to obtain unity PF. In this work, boost power factor correction (BPFC) has been made to operate in continuous conduction mode (CCM).

B. Load Adaptive PID-Aided Asymmetrical Voltage Cancellation Control Scheme

Now, to maintain a constant output voltage (or to improve dynamic behavior) across IH load 1 of FB-SRI, LA PID-aided AVC control scheme has been developed. Fig. 4(a) shows a complete block diagram of

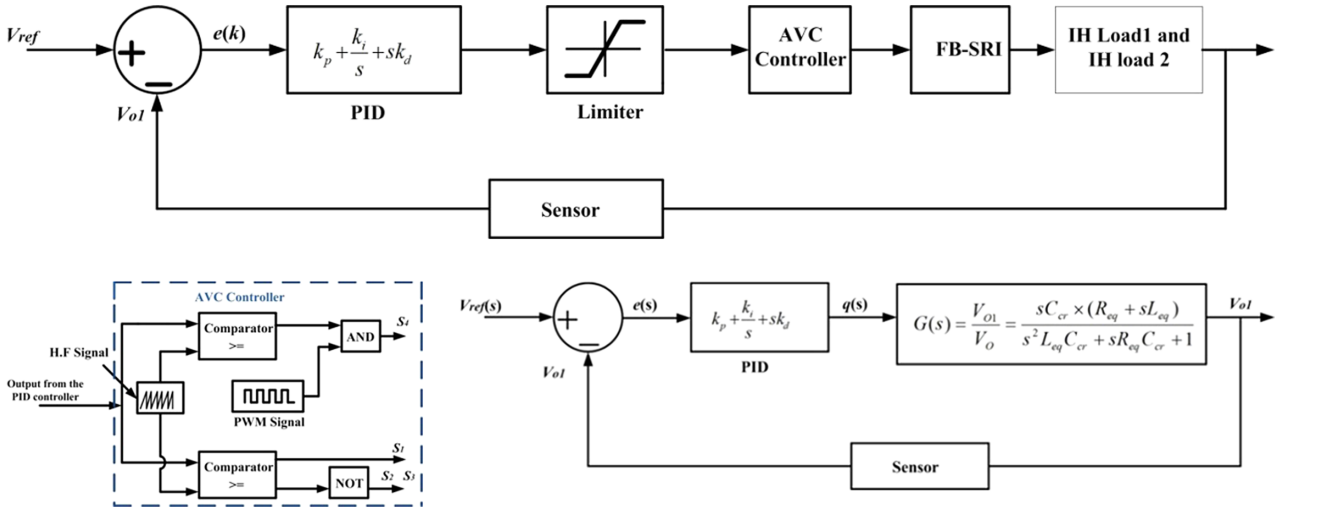

Fig. 4. PID-aided asymmetrical voltage cancellation (AVC) control scheme-based induction heating (IH) system. Block diagram, AVC control scheme, and plant model. FB-SRI, full-bridge series resonant inverter.

PID-aided AVC control scheme. Firstly, the output voltage (V_{o1}) across load 1 has been sensed and compared with the reference voltage (V_{ref}). After that, the generated error ($e(k)$) between V_{o1} and V_{ref} is corrected through a PID controller. The generated error between V_{o1} and V_{ref} in discrete domain is as follows:

$$e(k) = V_{ref}(k) - V_o(k) \tag{9}$$

$$\Delta e(k) = e(k) - e(k-1) \tag{10}$$

where $\Delta e(k)$, $e(k)$, and $e(k-1)$ are the change in error, error at kth, and error at $(k-1)$th moments, respectively.

The output of a PID controller is given to the limiter which is used to avoid shoot-through duty ratio from exceeding a predefined threshold. Finally, AVC is employed to generate PWM pulses for FB-SRI as shown in Fig. 4(b). The plant model for the proposed control scheme is shown in Fig. 4(c). The complete transfer function of shown plant model is evaluated in order to design the controller which is as follows:

$$\frac{V_{o1}(s)}{V_{ref}(s)} = \frac{(k_p + k_i/s + sk_d)\times sC_{cr}(R_{eq} + sL_{eq})/(s^2L_{eq}C_{cr} + sR_{eq}C_{cr} + 1)}{1 + (k_p + k_i/s + sk_d)\times sC_{cr}(R_{eq} + sL_{eq})/(s^2L_{eq}C_{cr} + sR_{eq}C_{cr} + 1)} \tag{11}$$

On solving (11),

$$\frac{V_{o1}(s)}{V_{ref}(s)} = \frac{(s^2k_d + sk_p + k_i)\times C_{cr}(R_{eq} + sL_{eq})}{(s^2L_{eq}C_{cr} + sR_{eq}C_{cr} + 1) + (s^2k_d + sk_p + k_i)\times C_{cr}(R_{eq} + sL_{eq})} \tag{12}$$

To perform the dynamic study, initially IH load 2 (modeled as R_{eq2} and L_{eq2}) is assumed OFF, and after some instant of time, it is connected parallel to IH load 1 (modeled as R_{eq1} and L_{eq1}) through unit step response. Whenever IH load 2 is connected (which is parallel to IH load 1) to load 1, the effective voltage across load 1 gets decreased. So the main objective of this controller is to keep constant effective voltage (within reasonable limit) across IH load 1 in order to get uniform heating effect.

III. STEADY-STATE ANALYSIS OF CONVERTERS

The steady-state analysis of boost PFC converter and FB-SRI has been done by assuming the normal operation of these converters which is as follows.

A. Boost Power Factor Correction Converter

The primary function of this converter is to improve the power factor of utility mains as well as to protect from HF EMI effect. In order to ensure minimum current ripple and to protect from HF current, CCM is assumed for the operation of this converter. The key waveform for a BPFC converter in CCM mode is shown in Fig. 5 in which D is the duty cycle, T_{sb} is the switching time period of switch S_b, I_L is the average inductor current, and V_{DCl} is the average dc link voltage. The average voltage across the inductor can be assumed zero. Thus,

$$V_{DC}DT_{sb} + (V_{DC} - V_{DCl})(1-D)T_{sb} = 0 \tag{13}$$

where V_{DC} is the DC voltage after rectification and V_{DCl} is the DC link voltage or boost voltage after boost operation.

Now, on solving (13), voltage conversion ratio is obtained which is same as boost converter which is as follows.

$$\frac{V_{DCl}}{V_{DC}} = \frac{1}{1-D} \tag{14}$$

Change in the inductor current can be written as follows:

$$\Delta I_L = I_{L\max} - I_{L\min} = \frac{V_{DC}}{L_{in}}DT_{sb} \tag{15}$$

where I_{Lmax} and I_{Lmin} are the values of maximum and minimum inductor current, respectively, while switching operation. As a result of this, the temporal inductor current can be written as

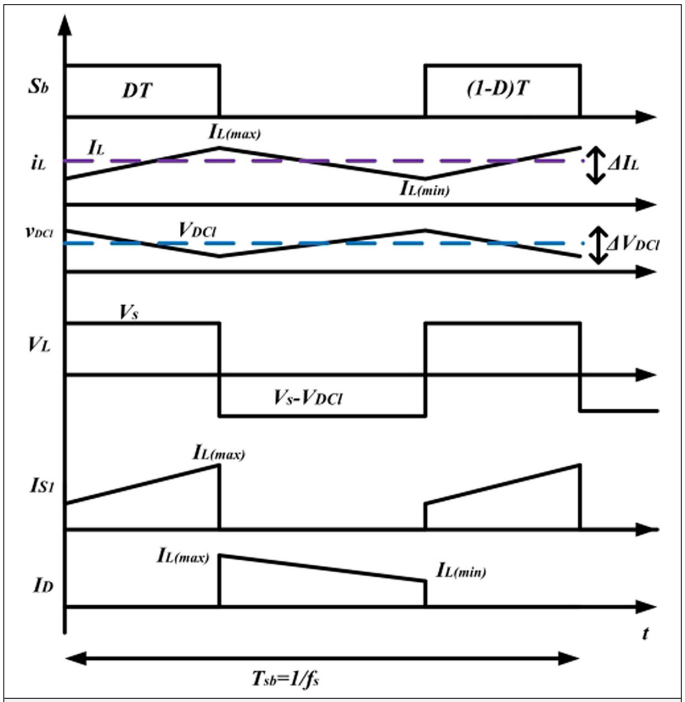

Fig. 5. Waveform of a BPFC converter in the continuous conduction mode mode.

$$I_L(t)=\begin{cases}\left(I_L-\dfrac{\Delta I_L}{2}\right)+\dfrac{\Delta I_L}{DT_{sb}}t,(0\le t<DT_{sb})\\ \left(I_L+\dfrac{\Delta I_L}{2}\right)-\dfrac{\Delta I_L}{DT_{sb}}(t-DT_{sb}),(DT_{sb}\le t<T_{sb})\end{cases} \tag{16}$$

To satisfy CCM condition by assuming unity PF operation,

$$\begin{aligned}&CCM\Rightarrow I_{L,0}>0\\ &\Rightarrow I_L>\frac{\Delta I_L}{2}\Leftrightarrow\frac{P_{DC}}{V_{DC}}>\frac{V_{DC}}{2L_{in}}DT_{sb}\end{aligned} \tag{17}$$

where P_{DC} is the DC input power for boost PFC converter.

Thus,

$$P_{DC}>\frac{V_{DC}^2}{2L_{in}}DT_{sb} \tag{18}$$

Consequently, the DC input power (P_{DC}) can be exchanged between V_{DC}, L_{in}, and modulating parameters D and T_{sb} to ensure CCM condition for a given supply voltage level.

B. Analysis of Full-Bridge Series Resonant Inverter Under Asymmetrical Voltage Cancellation Scheme

Considering a FB-SRI topology as shown in Fig. 1, Fig. 6(a) shows a generalized quasi-square wave output voltage. To control the voltage of this waveform, four control parameters (T_s, α_+, α_-, and β) are generally utilized. To enable AVC control scheme, α_- must be zero, and the obtained waveform is shown in Fig. 6(b). The average output power (P_o) of IH load 1 and load 2 can be controlled by controlling the angle α. Alternatively, with the consideration of an open-loop IH system, Fig. 6(c) shows the variation of output power across IH

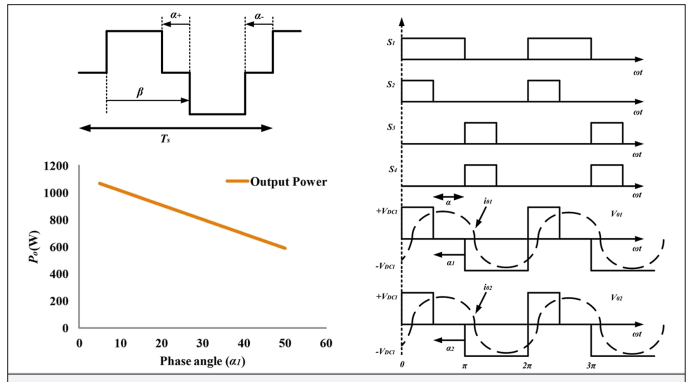

Fig. 6. Quasi-square voltage waveform. Output voltage waveforms using asymmetrical voltage cancellation scheme. Variation of output power (P_o) w.r.t. α_1.

load with the variation of controlling angle (α). In Fig. 6(b), V_{o1} and V_{o2} are the output voltage across IH load 1 and 2, respectively. The steady-state voltage across IH load 1 (V_{o1}) and IH load 2 (V_{o2}) can be determined as follows:

$$V_{o1}=v_{o1}+\sum_{n=1}^{\infty}\left\{A_n\cos n\omega_s t+B_n\sin\omega_s t\right\} \tag{19}$$

where

$$v_{o1}=\frac{1}{T}\int_0^T V_{o1}(t)d\omega_s t=\frac{(\pi-\alpha_1)V_{DCI}-\pi V_{DCI}}{2\pi}=\frac{-\alpha_1 V_{DCI}}{2\pi} \tag{20}$$

Since $a_n=0$

$$B_n=\frac{2}{T}\int_0^T V_{o1}(t)\sin n\omega_s t d\omega_s=\frac{V_{DCI}}{\pi}\sum_{n=1}^{\infty}\frac{1}{n}\left[-\cos(\pi-\alpha_1)-\cos n\pi\right]\sin n\omega_s t \tag{21}$$

Therefore,

$$V_{o1}=\frac{-\alpha_1 V_{DCI}}{2\pi}+\frac{V_{DCI}}{\pi}\sum_{n=1}^{\infty}\frac{1}{n}\left[-\cos(\pi-\alpha_1)-\cos n\pi\right]\sin n\omega_s t \tag{22}$$

Let $V_{mo1,n}$ is the maximum voltage across IH load 1 at the nth harmonic.

$$V_{mo1,n}=\frac{V_{DCI}}{\pi}\sum_{n=1}^{\infty}\frac{1}{n}\left[-\cos(\pi-\alpha_1)-\cos n\pi\right] \tag{23}$$

On considering lower order harmonics (i.e., $n=1$),

$$V_{m01,1}=\frac{V_{DCI}}{\pi}\left[1-\cos(\pi-\alpha_1)\right] \tag{24}$$

Fundamental load current (i_{o1}) across IH load 1,

$$i_{o1}=I_{m1}\sin(\omega_s t-\varphi_1) \tag{25}$$

Let, $I_{m1} = I_{mo1,1}$

$$I_{mo1,1} = \frac{V_{mo1,1}}{|Z_{eq1}|} = \frac{V_{DCI}\left[1-\cos(\pi-\alpha_1)\right]}{\pi R_{eq1}\sqrt{1+jQ^2\left(\omega_n - \frac{1}{\omega_n}\right)^2}} \quad (26)$$

Now, the average output power across IH load 1 can be derived as follows:

$$P_{o1} = I_{m1}^2 R_{eq1} = \frac{V_{DCI}^2\left[1-\cos(\pi-\alpha_1)\right]^2}{\pi^2 R_{eq2}\left[1+jQ^2\left(\omega_n - \frac{1}{\omega_n}\right)^2\right]} \quad (27)$$

By manipulating (27) using boost DC voltage (V_{DCI}) expression (14), the average output power for proposed IH system ($P_{o1,p}$) results as follows:

$$P_{o1,p} = \frac{\left(\frac{V_{DC}}{1-D}\right)^2 \times\left[1-\cos(\pi-\alpha_1)\right]^2}{\pi^2 R_{eq1}\left[1+jQ^2\left(\omega_n - \frac{1}{\omega_n}\right)^2\right]} \quad (28)$$

Similarly, power equations for IH load 2 can be written as follows:

$$P_{o2} = I_{m2}^2 R_{eq2} = \frac{V_{DCI}^2\left[1-\cos(\pi-\alpha_2)\right]^2}{\pi^2 R_{eq2}\left[1+jQ^2\left(\omega_n - \frac{1}{\omega_n}\right)^2\right]} \quad (29)$$

$$P_{o2,p} = \frac{\left(\frac{V_{DC}}{1-D}\right)^2 \times\left[1-\cos(\pi-\alpha_2)\right]^2}{\pi^2 R_{eq2}\left[1+jQ^2\left(\omega_n - \frac{1}{\omega_n}\right)^2\right]} \quad (30)$$

However, in the proposed IH system, the average output power is the combination of boost PFC circuit operation and the HF FB-SRI operation. So, if the duty cycle of boost PFC increases, the DC link voltage (V_{DCI}) also increases. This results in the increment of the output average power across the loads.

But, if the boost PFC converter will not apply, then only V_{DC} (output of bridge rectifier) will act as input for FB-SRI. In this case, the conventional average output power across IH load 1 ($P_{o1,C}$) can be written as follows:

$$P_{o1,C} = \frac{V_{DC}^2\left[1-\cos(\pi-\alpha_1)\right]^2}{\pi^2 R_{eq}\left[1+jQ^2\left(\omega_n - \frac{1}{\omega_n}\right)^2\right]} \quad (31)$$

At duty cycle, $D = 0.5$, the average output power ($P_{o1,p}$) in the proposed IH system becomes four times than the average output power ($P_{o1,C}$) in the conventional IH system (i.e., without a boost PFC converter). This is as follows:

$$\Rightarrow \frac{P_{o1,p}}{P_{o1,C}} = \frac{\left(\frac{V_{DC}}{1-D}\right)^2 \times\left[1-\cos(\pi-\alpha_1)\right]^2}{\pi^2 R_{eq}\left[1+jQ^2\left(\omega_n - \frac{1}{\omega_n}\right)^2\right]} \div \frac{V_{DC}^2 \times\left[1-\cos(\pi-\alpha_1)\right]^2}{\pi^2 R_{eq}\left[1+jQ^2\left(\omega_n - \frac{1}{\omega_n}\right)^2\right]} \quad (32)$$

Therefore,

$$\frac{P_{o1,p}}{P_{o1,C}} = \frac{1}{(1-D)^2} \quad (33)$$

At $D = 0.5$,

$$P_{o1,p} = 4P_{o1,C} \quad (34)$$

So, (34) concludes that the proposed IH system yields more power as compared to the conventional IH system.

IV. PERFORMANCE EVALUATION OF THE PROPOSED INDUCTION HEATING SYSTEM USING SIMULATION RESULTS

To evaluate the performance of the proposed IH system for two loads, simulation is carried out using MATLAB/Simulink environment. As aforesaid, a boost PFC converter has been used as front-end converter, and then an FB-SRI is employed in order to ensure unity PF operation and generate HF AC, respectively. The designed parameters for the simulation are divided into two sides, that is the boost PFC converter side and the FB-SRI side, which is given in Table I. The utility supply voltage (V_s) is kept at 230 V and 50 Hz. The

TABLE I. PARAMETERS USED FOR SIMULATION

Boost PFC Converter Side			**High-Frequency FB-SRI Side**			
Simulation Parameters	**Symbol**	**Value**	**Simulation Parameters**		**Symbol**	**Value**
Input voltage	V_{in}	230 $V_{r.m.s}$, 50 Hz	Common resonating capacitor		C_{cr}	0.8 uF
Average rectified voltage	V_{DC}	207 V	IH load 1	Equivalent resistance	R_{eq1}	5 Ω
				Equivalent inductance	L_{eq1}	52.7 uH
Boost PFC inductor	L_{in}	0.01 H	IH load 2	Equivalent resistance	R_{eq2}	40 Ω
				Equivalent inductance	L_{eq2}	52.7 uH
DC link capacitor	C	0.02 F	Switching frequency		f_s	25 kHz
DC link voltage	V_{DCI}	330 V	Output power		P_0	1.2 kW

FB-SRI, full-bridge series resonant inverter; PFC, power factor correction.

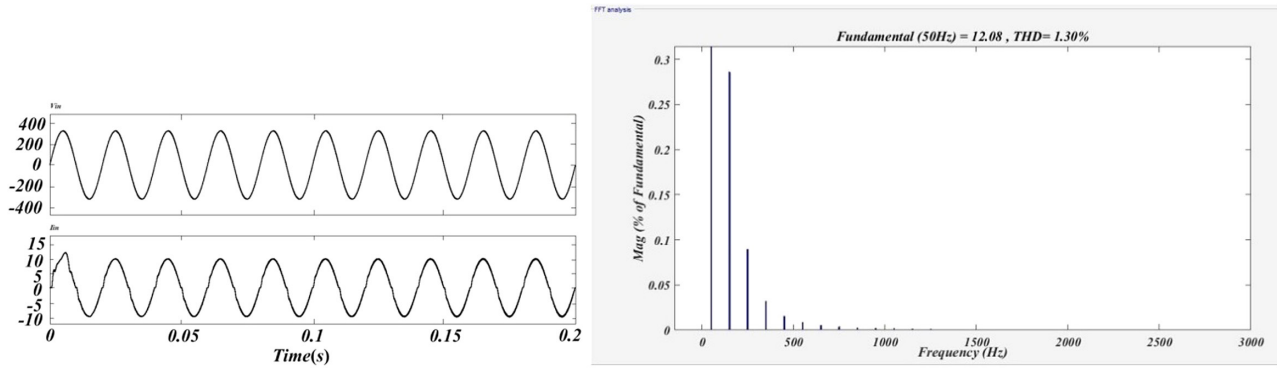

Fig. 7. Simulation results.

applied input average voltage for boost PFC converter is 207 V (0.9 × $V_{r.m.s}$, output of diode bridge rectifier) which gives the DC link voltage (V_{DCl}) of 330 V.

The simulation results of input voltage (V_s), input current (I_s), and THD are shown in Fig. 7, having the values of 225 V, 7.07 A, and 1.30%, respectively. Also, the PF (between V_s and I_s) of "I_s" using a BPFC converter was found to be unity. This less value of PF and THD shows the uniqueness of the proposed IH system using a boost PFC converter. Also, it can be concluded that there is no HF component in the input current (I_s), which generally comes from the HF inverter side. Owing to this good PF and low THD, IH load can extract more power from the utility mains. The DC link voltage (V_{DCl}) which has been generated through boost PFC is shown in Fig. 8, and it has been fed to the FB-SRI. The magnitude of V_{DCl} was found to be 330 V which is boost in nature.

Now, to evaluate the dynamic performance of proposed LA PID-aided AVC control-based IH system, two loads have been assumed, IH load 1 and 2. Initially, IH load 2 has been kept OFF, but when this load is connected to load 1, the effective voltage across the load 1 decreased. The output across IH load 1 of the proposed IH system is being regulated through a proposed control algorithm, and it can be represented by putting the parameters of R_{eq1}, L_{eq1}, and C_{cr} (as in Table I) in (12), which is as follows:

$$V_{o1}(s)=\frac{(s^2k_d+sk_p+k_i)\times 0.8\times 10^{-6}(5+s52.7\times 10^{-6})}{(s^2 52.7\times 0.8\times 10^{-12}+s5\times 0.8\times 10^{-6}+1)+(s^2k_d+sk_p+k_i)\times s0.8\times 10^{-6}(5+s52.7\times 10^{-6})}\times V_{ref}(s) \quad (35)$$

where k_p, k_i, and k_d are the proportional, integral, and derivative constants, respectively. The design of these constants has been done through Ziegler and Nichols technique [31]. This approach starts by setting the integral and differential gains to zero before increasing the proportional gain until the system becomes unstable. Consequently, k_p, k_i, and k_d are calculated as $0.6k_{max}$, $2.0f_o$, and $0.125/f_o$, respectively. Here, k_{max} is the value of k_p at the point of instability, and f_0 is the frequency of the oscillation. For the simulation study, IH load 2 is aided to load 1 at 0.4 s by using a unit step response as shown in Fig. 2. As a result of this, the output voltage across load 1 suddenly decreased to 85 V from its reference voltage of 100 V at 0.4 s, but due to proposed controller, the IH system again restores the voltage across load 1 to its normal voltage of 99.7 V (i.e., close to the reference voltage) at 0.48 s. Along with this, the output current through IH load 1 is also decreased by 0.98 A at 0.4 s and again achieved to its normal value at 0.48 s. At the same time, the total HF current ($I_{out(HFAC)}$) increased between the time period of 0.4 s and 0.48 s to satisfy the load demand, as shown in Fig. 9. Thus, it can be concluded that the time taken by the proposed controller to achieve normal value is 0.08 s. Voltage and current are in same phase because of the resonating operation of FB-SRI. This dynamic behavior of output voltage and current is shown in Fig. 10. The encircled part in Fig. 10(a)shows the zoom view of waveform.

The switching frequency (f_s) for HF FB-SRI is kept at 25 kHz, and it is calculated by using series resonance condition which is as follows:

$$f_r=\frac{1}{2\pi\sqrt{L_{eq1}(orL_{eq2})C_{cr}}} \quad (36)$$

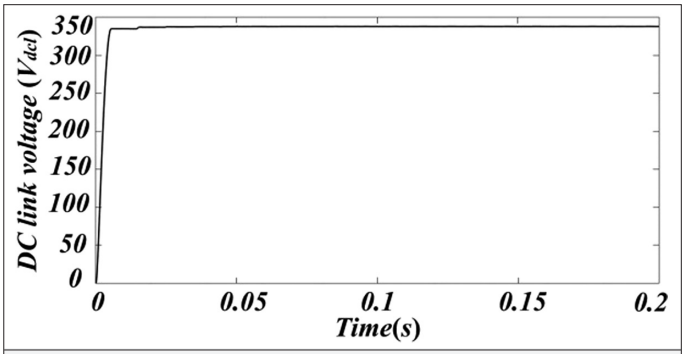

Fig. 8. DC link voltage (V_{DCl}).

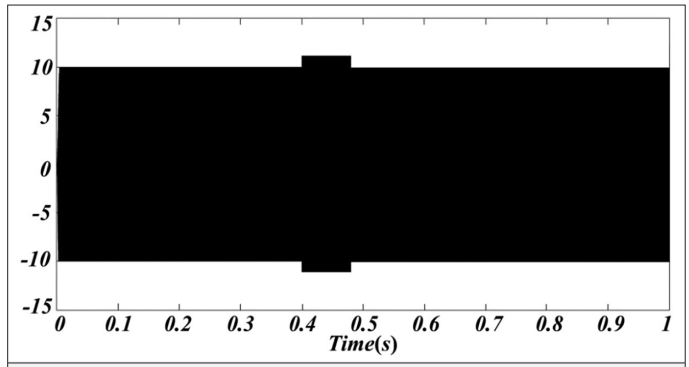

Fig. 9. Total high-frequency current ($I_{out(HFAC)}$).

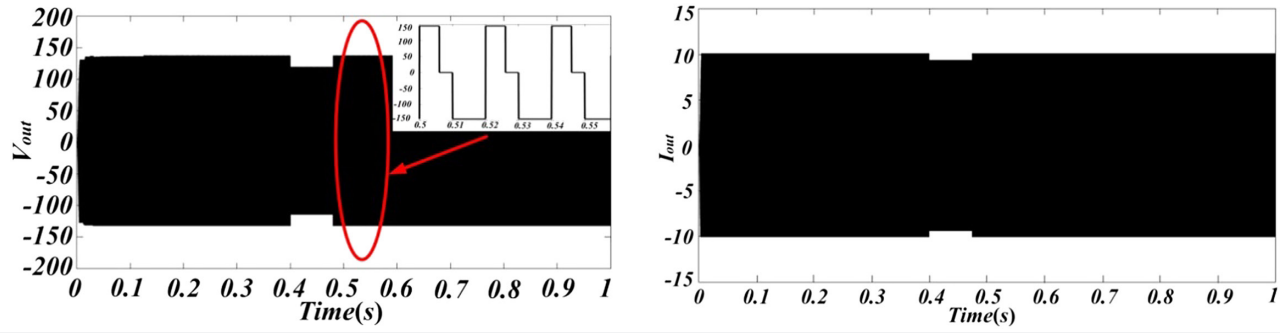

Fig. 10. Dynamic response of output voltage (V_{out}) and current (I_{out}) across induction heating load 1.

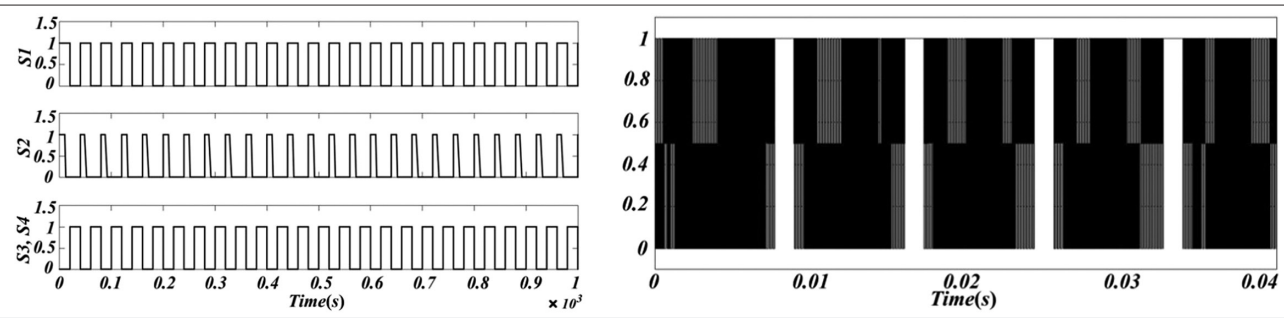

Fig. 11. Pulse width modulation pulses.

As per (36), the calculated resonant frequency (f_r) was found to be 24.5 kHz, but to enable ZVS condition, the switching frequency (f_s) is kept at 25 kHz. The HF pulses for HF FB-SRI and boost PFC switch (S_b) generated from the proposed controller are shown in Fig. 11(a) and (b).

As from the simulation results obtained, it can be concluded that the proposed controller maintains constant voltage profile in one load due to effect of another IH load. Also, during dynamic operation, the proposed IH system for dual load maintains the unity PF with low THD. As a consequence, this controller can be extended to multi-load IH systems.

V. EXPERIMENTAL PROTOTYPE AND ITS RESULTS

An experimental 1.2 kW system prototype has been developed, as shown in Fig. 12, to test the real-time operation and assess the performance of the proposed IH system. The supply system for IH loads comprised of a bridge rectifier, a boost converter, and an FB-SRI. A bridge rectifier has been developed using four diodes having a current rating of 10 A. After that, a boost PFC converter has been made using the switch IRF640, a diode, an inductor of 0.01 H, and a capacitor of 0.02 F. Finally, to generate HF AC, an FB-SRI has been deployed which has been built using the switch IRF640. Induction heating load has been developed using Litz wire having a diameter of 14 cm. A resistive load was connected in parallel to the IH load using a single-pole double-throw switch in order to change the load for the dynamic study of the proposed controller. The parameters for the design of the experimental setup are approximately the same as simulation parameters. Fig. 13 shows the experimental results for the input voltage, input current, and steady-state DC link voltage (generated from the boost PFC converter) having a magnitude of 220 V, 50 Hz, 7 A, and 330 V_{DC}, respectively. This indicates the approximately

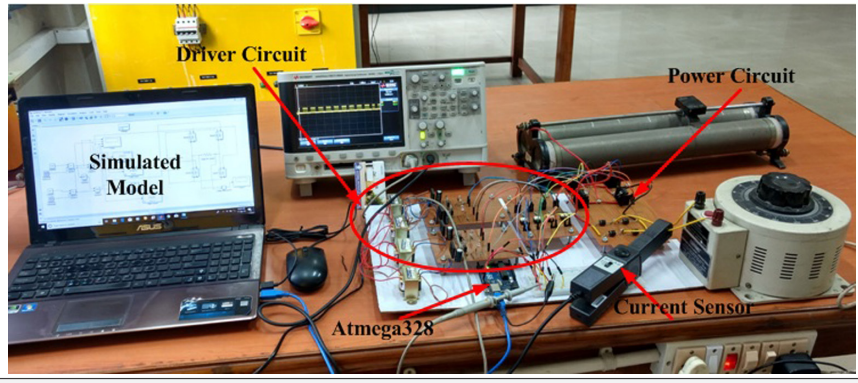

Fig. 12. Experimental setup of a power supply system for the induction heating system.

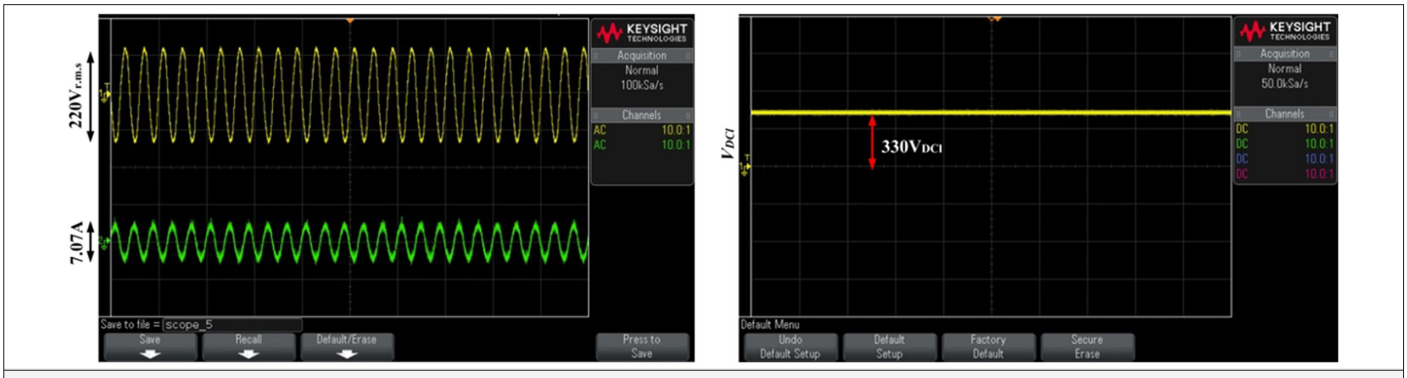

Fig. 13. Experimental results.

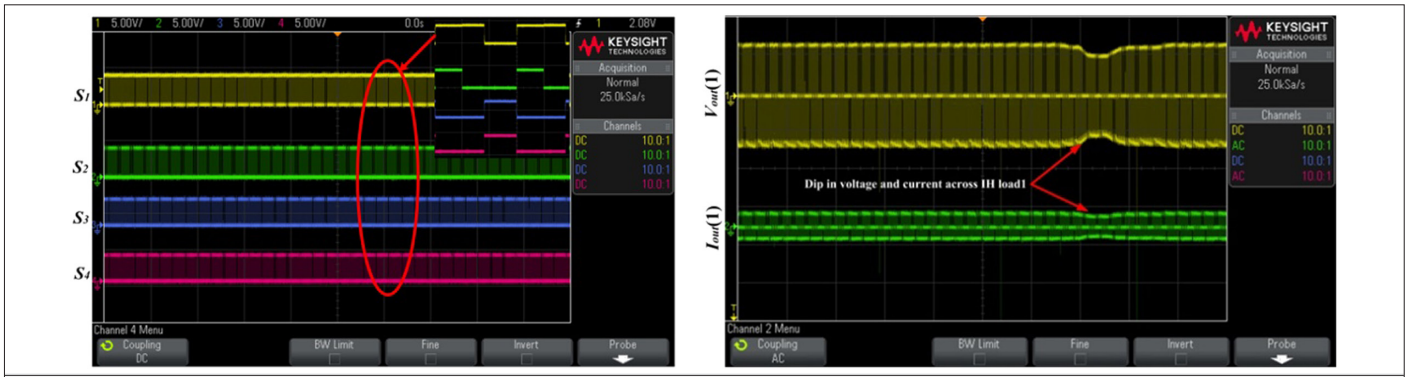

Fig. 14. Experimental results of pulse width modulation pulses and output voltage and current.

unity PF (that is 0.985) operation and less HF component in the input current waveform of the proposed IH system using a boost PFC converter. The proposed control algorithm for a boost PFC converter and FB-SRI for dual IH loads is implemented using MATLAB/Simulink environment, and the code for these algorithms has been downloaded into Arduino Atmega328. The TLP250 opto-isolator circuit, which isolates between high-power and low-power control circuits, is used to drive the pulses generated by the Arduino atmega326. The amplified pulses generated from the driver circuit are given to boost switch (S_b) and FB-SRI switches (S_1–S_4). The experimental validation of pulses is shown in Fig. 14(a) where the encircled part shows the expandable view of this HF pulses. The experimental waveforms of the HF output voltage (V_{out}) and current (I_{out}) across IH load 1 are shown in Fig. 14(b), which validates the dynamic response of the proposed IH system for dual loads as obtained in the simulation result. It can be observed from the experimental results that the proposed control algorithm maintains the reference voltage across IH load 1 (V_{ref}=100 *V*) according to the IH load 2. This voltage and current have been recorded using Infiniivison DSO-X 2022 A digital storage oscilloscope of 200 MHz. The load current has been measured using the TEKTRONIX A622 AC/DC current probe. The expanded view of HF output voltage (V_{out}), i.e., AVC waveform, is shown in Fig. 15(a). Also, efficiency has been measured at different output power levels, as shown in Fig. 15(b). From this graph, the obtained efficiency was approximately 81%.

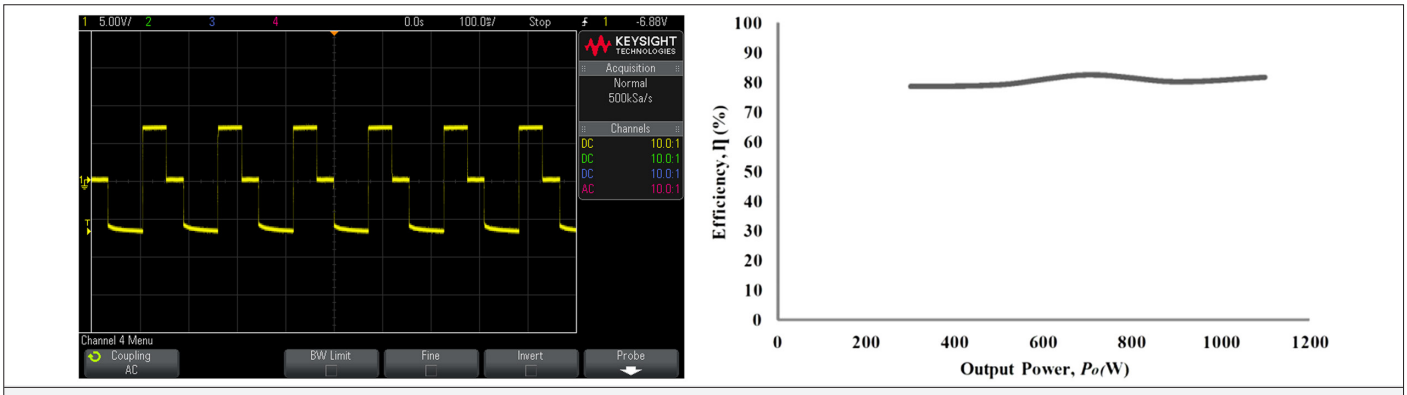

Fig. 15. Experimental results of the output voltage in expanded form and efficiency.

As a result of this, the simulation and experimental results confirm that a boost PFC converter-based IH system using the proposed control algorithm for dual IH loads guarantees improvement in the PF, ensures protection from HF component in the line current, improves dynamic response, and maintains constant output voltage across IH load. Furthermore, the proposed control strategy for a boost PFC converter and an HF FB-SRI is simple and robust.

VI. CONCLUSION

In this paper, a LA PID-aided AVC control scheme has been developed for the HF FB-SRI for the dual loads, followed by a boost PFC converter. This controller maintains the constant output voltage profile across IH load 1 when IH load 2 is suddenly connected to IH load 1. In addition to this, a boost PFC converter has been used as a front-end converter to enable the unity PF operation of the proposed IH system. Also, mathematical analysis for the output power has been established, which proves that the proposed IH system can yield more power as compared to the conventional IH system. Proposed controllers have been designed using a digital controller (Arduino Atmega 3280). The switching frequency for an FB-SRI is kept at higher than calculated resonant frequency to enable the ZVS condition which reduces the power losses across the switches. The simulation results were tested using the experimental setup of 1.2 kW HF FB-SRI, which proves the uniqueness and feasibility of this proposed IH system for dual loads. This controller can be extended to multi-load IH systems, and also intelligent controllers like model predictive controllers can be used in future for better improvement in dynamic response.

Peer-review: Externally peer-reviewed.

Author Contributions: Concept – A.K.; Design – A.K., C.K.; Supervision – A.K.; Analysis and/or Interpretation – A.K., C.K.; Literature Review – C.K.; Writing – A.K., C.K.; Critical Review – A.K.

Declaration of Interests: The authors have no conflicts of interest to declare.

Funding: The authors declared that this study has received no financial support.

REFERENCES

1. O. Lucia, P. Maussion, E. J. Dede, and J. M. Burdio, "Induction heating technology and its application: Past developments, current technology and future challenges," *IEEE Trans. Ind. Electron.*, vol. 61, no. 5, pp. 2509–2520, 2014. [CrossRef]
2. P. R. Stauffer, T. C. Cetas, and R. C. Jones, "Magnetic induction heating of ferromagnetic implants for inducing localized hyperthermia in deep seated tumors," *IEEE Trans. Bio Med. Eng.*, vol. 31, no. 2, pp. 235–251, 1984. [CrossRef]
3. W. Han, K. T. Chau, and W. H. Lam, "All-utensil domestic induction heating system," *Energy Convers. Manag.*, vol. 195, pp.1035–1043, 2019. [CrossRef]
4. K. Sayed, F. Abo-Elyousr, F. N. Abdelbar, and H. El-zohri, "Development of series resonant inverters for induction heating applications," *Eur. J. Eng. Res. Sci.*, vol. 3, no. 12, pp. 36–39, 2018. [CrossRef]
5. K. Neogi *et al.*, "A new approach for the stability analysis of high-frequency series resonant inverter-fitted induction heater," *Ain Shams Eng. J.*, vol. 10, no. 1, pp.185–194, 2019. [CrossRef]
6. A. Kumar, D. Sarkar, and P. K. Sadhu, "An efficient power control technique for high-frequency resonant inverter in induction heating system," *Eng. Technol. Appl. Sci. Res.*, vol. 8, no. 6, pp. 3530–3535, 2018. [CrossRef]
7. P. Vishnuram, S. Ramasamy, P. Suresh, and A. S. kumar, "A simple digital control for mitigating voltage stress on single switch resonant inverter for induction cooking applications," *Int. J. Electron. Lett.*, vol. 8, no. 2, 162–169, 2020. [CrossRef]
8. O. Lucia, J. M. Burdio, I. Millan, J. Acero, and D. Puyal, "Load-adaptive control algorithm of half-bridge series resonant inverter for domestic induction heating," *IEEE Trans. Ind. Electron.*, vol. 56, no. 8, pp. 3106–3116, 2009. [CrossRef]
9. S. Yin, X. Ma, C. Luo, J. Wang, and X. Zhu, "Modeling and analysis of transient performance for induction heating system considering frequency-dependent inductive load," *IEEE Trans. Magn.*, vol. 55, no. 6, pp. 1–4, 2019. [CrossRef]
10. C. Carretero, O. Lucia, R. Alonso, and J. M. Burdio, "Frequency dependent modelling of domestic induction heating using numerical methods for accurate time-domain simulation," *IET Power Electron.*, vol. 5, no. 8, pp. 1291–1297, 2012.
11. J. Acero, C. Carretero, R. Alonso, and J. M. Burdio, "Quantitative evaluation of induction efficiency in domestic induction heating applications," *IEEE Trans. Magn.*, vol. 49, no. 4, pp. 1382–1389, 2013. [CrossRef]
12. T. Mishima, S. Sakamoto, and C. Ide, "ZVS phase-shift PWM-controlled single-stage boost full-bridge AC–AC converter for high-frequency induction heating applications," *IEEE Trans. Ind. Electron.*, vol. 64, no. 3, pp. 2054–2061, 2017. [CrossRef]
13. O. Lucia, J. M. Burdio, I. Millan, J. Acero, and L. A. Barragan, "Efficiency-oriented design of ZVS half-bridge series resonant inverter with variable frequency duty cycle control," *IEEE Trans. Power Electron.*, vol. 25, no. 7, pp. 1671–1674, 2010. [CrossRef]
14. V. Esteve *et al.*, "Improving the efficiency of IGBT series-resonant inverters using pulse density modulation," *IEEE Trans. Ind. Electron.*, vol. 58, no. 3, pp. 979–987, 2011. [CrossRef]
15. O. Lucia, J. M. Burdio, L. A. Barragan, C. Carretero, and J. Acero, "Series resonant multiinverter with discontinuous-mode control for improved light-load operation," *IEEE Trans. Ind. Electron.*, vol. 58, no. 11, pp. 5163–5171, 2011. [CrossRef]
16. N. A. Ahmed, "High-frequency soft-switching ac conversion circuit with dual-mode PWM/PDM control strategy for high-power IH applications," *IEEE Trans. Ind. Electron.*, vol. 58, no. 4, pp. 1440–1448, 2010. [CrossRef]
17. N. J. Park, D. Y. Lee, and D. S. Hyun, "A power-control scheme with constant switching frequency in class-D inverter for induction-heating jar application," *IEEE Trans. Ind. Electron.*, vol. 54, no. 3, pp. 1252–1260, 2007. [CrossRef]
18. P. Vishnuram, S. Ramasamy, P. Suresh, and A. Sureshkumar, "Phase-locked loop-based asymmetric voltage cancellation for the power control in dual half-bridge series resonant inverter sharing common capacitor for induction heating applications," *J. Control Autom. Electr. Syst.*, vol. 30, no. 6, pp. 1094–1106, 2019. [CrossRef]
19. M. B. Borage, K. V. Nagesh, M. S. Bhatia, and S. Tiwari, "Characteristics and design of an asymmetrical duty-cycle-controlled LCL-T resonant converter," *IEEE Trans. Power Electron.*, vol. 24, no. 10, pp. 2268–2275, 2009. [CrossRef]
20. O. Lucia, J. Acero, C. Carretero, and J. M. Burdio, "Induction heating appliances: Toward more flexible cooking surfaces," *IEEE Ind. Electron. Mag.*, vol. 7, no. 3, pp. 35–47, 2013. [CrossRef]
21. F. Forest, S. Faucher, J. Y. Gaspard, D. Montloup, J. J. Huselstein, and C. Joubert, "Frequency-synchronized resonant converters for the supply of multiwinding coils in induction cooking appliances," *IEEE Trans. Ind. Electron.*, vol. 54, no. 1, pp. 441–452, 2007. [CrossRef]
22. A. Kumar, R. Raman, and P. K. Sadhu, "Dynamic behavior improvement of induction heating converters using fuzzy logic controller," *Rev. Roum. Sci. Tech. S. Electrotechn. Energ.*, vol. 64, no. 2, pp. 163–168, 2019.
23. P. Kongsakorn, and A. Jangwanitlert, "A two-output high frequency series-resonant induction heater," in ECTI-CON2010: The 2010 ECTI International Conference on Electrical Engineering/Electronics, Computer, Telecommunications and Information Technology. IEEE Publications, Thailand, 2010, pp. 842–845.
24. K. L. Nguyen, O. Pateau, S. Caux, P. Maussion, and J. Egalon, "Robustness of a resonant controller for a multiphase induction heating system," *IEEE Trans. Ind. Appl.*, vol. 51, no. 1, pp. 73–81, 2014. [CrossRef]
25. F. Sanz, C. Sagues, and S. Llorente, "Induction heating appliance with a mobile double-coil inductor," in IEEE Industry Application Society Annual Meeting. IEEE Publications, 2014, pp. 1–7. [CrossRef]
26. C. Carretero, O. Lucia, J. Acero, and J. M. Burdio, "Computational modeling of two partly coupled coils supplied by a double half-bridge resonant inverter for induction heating appliances," *IEEE Trans. Ind. Electron.*, vol. 60, no. 8, pp. 3092–3105, 2012. [CrossRef]

27. P. K. Nayak, H. P. Singh, K. Pandey, and S. K. Sinha, "Single area & two area multimachine load frequency control strategy," 4th International Conference on Recent Developments in Control., Automation & Power Engineering (RDCAPE). IEEE Publications, 2021. [CrossRef]
28. B. Meziane, and H. Zeroug, "Comprehensive power control performance investigations of resonant inverter for induction metal surface hardening," *IEEE Trans. Ind. Electron.*, vol. 63, no. 10, pp. 6086–6096, 2016. [CrossRef]
29. S. M. Madani, M. R. Amini, H. Atighechi, and M. Dolatshahi, "Quasi-parallel resonant DC-link inverter with a reduced switch voltage stress," *Energy Convers. Manag.*, vol. 52, no. 1, pp.590–595, 2011. [CrossRef]
30. B. Hekimoğlu, and S. Ekinci, "Optimally designed PID controller for a DC-DC buck converter via a hybrid whale optimization algorithm with simulated annealing," *Electrica*, vol. 20, no. 1, pp. 19–27, 2020. [CrossRef]
31. B. R. Copeland, "The design of PID controllers using Ziegler Nichols tuning," *Zieglar-Nicholos Method*, 2008.

Dr. Anand Kumar was born in Bokaro, Jharkhand, India in 1991. He received his BE degree in Electrical and Electronics Engineering from the Rajiv Gandhi Technological University, Bhopal, Madhya Pradesh, India, in 2012 and his ME degree in Power Electronics (Electrical Engineering) from the Birla Institute of Technology, Mesra, Ranchi, India, in 2014. He has completed his PhD from the Indian Institute of Technology (Indian School of Mines), Dhanbad, India. He is presently working as an Assistant Professor in the Department of Electrical and Electronics Engineering at Sarala Birla University, Ranchi, India. Also, he served as an Assistant Professor in the Department of Electrical Engineering at Guru Gobind Singh Educational Society Technical Campus (GGSESTC), Kandra, Bokaro, India. He has several journal and conference publications at the national and international levels. He is a reviewer for various international journals of repute like IEEE Access, Electrica, and IEEE conferences. His research interests include power electronics converters, HF resonant converters, direct AC–AC converters, applications of resonant converter in domestic as well as industrial IH systems. He is available at anandsingh 1025@gmail.com, anand.kumar@sbu.ac.in.

Mr. Chandan Kumar was born in Ranchi, Jharkhand, India in 1986. He received his BE in Electronics and Instrumentation Engineering from the Dr. MGR University, Chennai, Tamil Nadu, India in 2009 and his ME degree in Control System (Electrical Engineering) from the Birla Institute of Technology, Mesra, Ranchi, India, in 2016. He has several years of industrial and teaching experience. Presently, he is pursuing a PhD from Sarala Birla University, Ranchi, Jharkhand, India. His research interests include sliding mode control system, second-order sliding mode control system, resonant inverters, and their applications in IH technology. He is available at chandankumarsingh31@gmail.com, chandan.kumar@sbu.ac.in.